A Single Antenna Full-Duplex Radio Using a Non-Magnetic, CMOS Circulator with In-built Isolation Tuning

Aravind Nagulu, Tingjun Chen, Gil Zussman, and Harish Krishnaswamy Department of Electrical Engineering, Columbia University, New York, NY 10027, USA (Invited Paper)

Abstract—Wireless systems which can simultaneously transmit and receive (STAR) are gaining significant academic and commercial interest due to their wide range of applications such as full-duplex (FD) wireless communication and FMCW radar. FD radios, where the transmitter (TX) and the receiver (RX) operate simultaneously at the same frequency, can potentially double the data rate at the physical layer and can provide many other advantages in the higher layers. The antenna interface of an FD radio is typically built using a multi-antenna system, or a single antenna through a bulky magnetic circulator or a lossy reciprocal hybrid. However, recent advances in CMOS-integrated circulators through spatio-temporal conductivity modulation have shown promise and potential to replace traditional bulky magnetic circulators. However, unlike magnetic circulators, CMOS-integrated non-magnetic circulators will introduce some nonlinear distortion and spurious tones arising from their clock circuitry. In this work, we present an FD radio using a highly linear CMOS integrable circulator, a frequency-flat RF canceler, and a USRP software-defined radio (SDR). At TX power level of $+15\,\mathrm{dBm}$, the implemented FD radio achieves a self-interference cancellation (SIC) of +55 dB from the circulator and RF canceler in the RF domain, and an overall SIC of $+95 \, dB$ together with SIC in the digital domain. To analyze the non-linear phenomena of the CMOS circulator, we calculated the link level data-rate gain in an FD system with imperfect SIC and then extended this calculation to count the effect of TX-RX non-linearity of the circulator. In addition, we provide a qualitative discussion on the spurious tone responses of the circulator due to the clocking imperfections and non-linearity.

Index Terms—Circulator, CMOS, conductivity modulation, full-duplex, non-reciprocity, self-interference cancellation.

I. INTRODUCTION

Traditional wireless systems are half-duplex (HD), where the transmission and reception of radio signals are separated in either different time slots (e.g., time-division duplexing, TDD). Another common approach is to use different frequency bands for the transmitter (TX) and the receiver (RX) (e.g., frequency division duplexing, FDD). In-band full-duplex (FD) wireless is an emerging wireless communications paradigm which allows simultaneous transmission and reception at the same frequency, and has the potential to improve the spectral efficiency at the physical (PHY) layer and to provide many other benefits at the higher layers [1]–[5]. Therefore, FD can possibly be applied to many applications including PHY layer security [6], relaying and forwarding [7], [8], and network localization [2], [6].

The fundamental challenge associated with FD wireless is the tremendous amount of self-interference (SI) leaking from the TX into the RX, which needs to be canceled to successfully receive the desired signal. This is usually achieved through SI suppression at the antenna interface and the self-interference cancellation (SIC) in the RF/analog and digital domains. At the antenna interface, the SI can be suppressed by using multi-antenna systems (separated TX and RX antennas) [9], [10], or a single antenna shared through a circulator [4], [11], [12] or a reciprocal hybrid such as the electrical balance duplexer [13], [14]. In addition, practical levels of SIC in the RF and digital domains have been demonstrated using off-the-shelf components or integrated circuits (ICs) [4], [10]-[12], [15], [16]. A traditional approach to realize circulators is to use ferrite materials biased by an external magnetic field. However, ferrite materials are not compatible with existing CMOS and, therefore, lead to large form-factors and high implementation cost.

Recent advances in CMOS-integrated circulators through time modulation [17]–[19] has shown potential to replace the bulky magnetic circulators. In this work, we present an FD radio using a highly linear CMOS circulator [17] and a USRP2 software-defined radio (SDR), which achieves high TX power handling of up to +16 dBm (limited by overall SIC) and +95 dB overall SIC across the antenna, RF, and digital domains. We also analyze the effects of the circulator TX-RX non-linearity on the achievable SIC. In addition, we provide a conceptual illustration on the spurious tone response of the circulator caused due to non-idealities and clocking imperfections.

The rest of the paper is organized as follows. Section II discusses the concept of spatio-temporal conductivity modulation (STCM), and the implementation of a highly-linear non-magnetic CMOS circulator with on-chip loss-free and inductor-free isolation tuning. Section III presents the implementation details of the FD radio built using the CMOS circulator. Here we also discussed the spurious tone response of the circulator and the effect of circulator's TX-RX non-linearity on overall SIC. Measurement results of the FD radio are presented in Section IV. Finally, Section V concludes the paper.

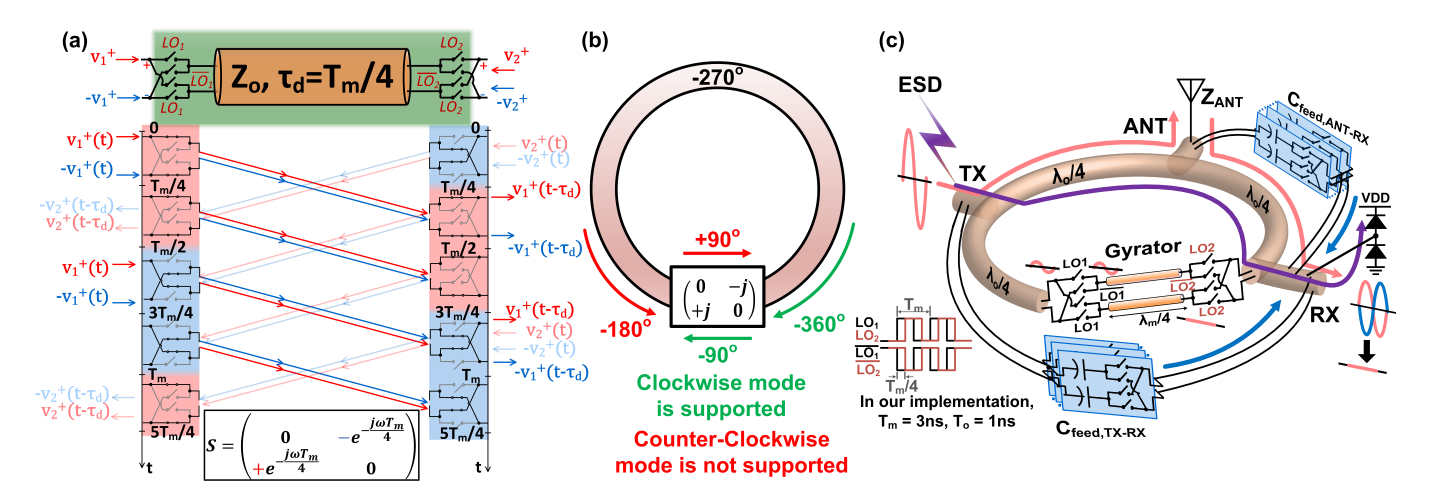


Fig. 1. (a) Time domain operation of the ultra-wideband gyrator. (b) Non-reciprocal circular ring supporting only clockwise mode propagation. (c) Circulator concept, including inductor-free, loss-free antenna balancing and design for high TX-power handling.

II. A CMOS MAGNETLESS NON-RECIPROCAL CIRCULATOR WITH LOSS-FREE, INDUCTOR-FREE ISOLATION TUNING

This section describes the architecture and implementation details of the non-magnetic circulator used in our FD radio prototype. The non-magnetic circulator is built using the concept of *synchronized spatio-temporal conductivity modulation (STCM) around transmission lines* [20], [21].

A. An Ultra-Broadband Gyrator Based on STCM around Transmission Lines

The gyrator element consists of a differential transmission line with a characteristic impedance equal to the differential port impedance, which is sandwiched between two doubly-balanced switch sets as shown in Fig. 1(a). The modulation signal of the right-hand-side switches is delayed with respect the left hand-side-switches by a value of $T_m/4$, which is quarter period of the modulation signal, and also the propagation delay of the transmission line. In this configuration, as illustrated in the time domain bounce diagram in Fig. 1(a), the signal traveling in the forward direction (left to right) experiences the delay of the transmission line, $T_m/4$. In the reverse direction (right to left), the signal experiences the delay of the transmission line with an additional sign flip. This additional sign flip in the reverse direction creates a ultra-broadband non-reciprocal phase shift of 180°, resulting in an ultra-broadband gyrator. The gyrator is postulated as a fifth fundamental circuit element [22] after resistor, capacitor, inductor, and transformer, and is considered as the basic building block for designing an arbitrary non-reciprocal circuit.

B. Architecture of the CMOS Circulator

This phase non-reciprocity is converted into amplitude non-reciprocity by wrapping a $3\lambda/4$ line (-270°) phase response at signal frequency) around a gyrator with $+90^{\circ}$ and -90° phase response in forward and reverse directions respectively (Fig. 1(b)). A circulator is then created by

inserting 3 ports namely, TX, ANT, and RX, along the $3\lambda/4$ transmission line with $\lambda/4$ spacing as depicted in Fig. 1(c). While the ports can be placed anywhere along the transmission line, placing the RX port right next to the gyrator [23] protects the CMOS switches in the gyrator from large TX swing, and hence substantially increases the linearity of the circulator. In addition, the TX power handling of the circulator has been improved due to the ultra-broadband gyrator architecture which allows lowering of the modulation frequency. For an operation frequency of 1 GHz, the switches in the gyrator were modulated at 333 MHz (1/3) of the signal frequency), thus enabling the use of the thick oxide 320 nm transistors with higher breakdown voltage, and consequently, higher power handling. This work notably improves linearity and power handling by 10–100× compared with our prior CMOS non-reciprocal circulators [23], [24], while compensating for a wide ANT impedance range.

C. In-built Isolation Tuning

TX-RX isolation of all shared-ANT interfaces is susceptible to antenna mismatches. The TX signal travels to the ANT port, and a portion of it gets reflected back due to the antenna mismatch and travels into the RX port. Typically, circulators are followed with antenna tuners but these introduce additional loss. In this work, a novel loss-free, inductor-free isolation tuning approach is proposed (Fig. 1), which leverages the inherent -90° phase shift in the TX-ANT path. A feedforward cancellation path consisting of a digitally-controlled capacitance bank is introduced from TX to RX, which injects a current that is -90° out of phase with the TX voltage due to its reactive nature, and is programmable in magnitude. Another such path is introduced from ANT to RX, and since the voltage at the ANT port is -90° out of phase with respect to the TX voltage, this path introduces a current which is in-phase with the TX signal. A differential circulator implementation enables sign inversion in each of these paths, and therefore complete coverage of the complex plane is enabled without inductors and resistors (i.e., additional

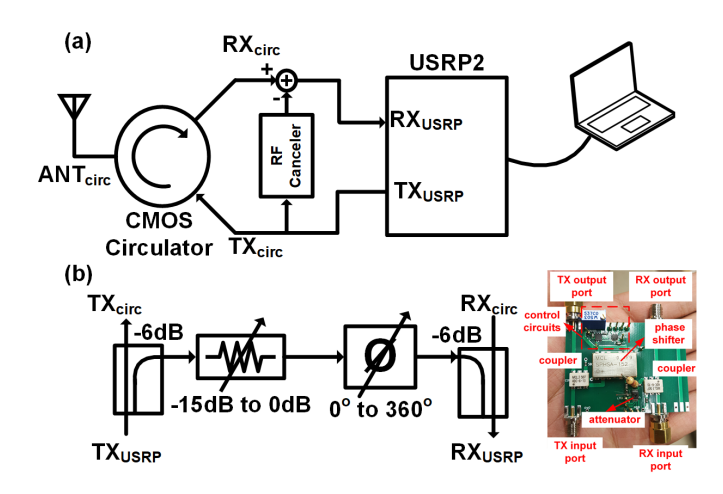


Fig. 2. (a) Block diagram of the FD radio prototype using CMOS circulator. (b) Block diagram of the frequency-flat amplitude- and phase-based RF canceller implemented using discrete components.

loss). In addition, the notch frequency of the isolation can be easily tuned by changing the tunable capacitor settings. The maximum isolation from this tuning technique is limited to $-55\,\mathrm{dB}$ by the resolution of the digitally-tunable switched capacitor banks.

The measured insertion losses of the circulator are 2.1/2.9 dB in the TX-ANT and ANT-RX paths, and ANT-RX noise figure is 3.1 dB. Using the tunable switched capacitor banks, >40 dB TX-RX isolation is achieved across the entire 1.85 ANT VSWR circle and beyond. The measured in-band TX-ANT/ANT-RX IIP3s are $+50.03\,\mathrm{dBm}$ and $+36.90\,\mathrm{dBm}$ respectively. TX-ANT input $P_{1\mathrm{dB}}$ is >+30.66 dBm (limited by the measurement setup), at which point the compression is only 0.66 dB, while the ANT-RX input $P_{1\mathrm{dB}}$ is +21.01 dBm. Measured TX-RX IIP3 is 24.22 dBm. Once tuned to +50 dB isolation at low TX power levels, the TX-RX isolation is >40 dB for TX powers up to +21.60 dBm. While the isolation can be tuned back for high TX powers, maintaining a decent isolation form low to high TX power is very critical in systems with large peak-to-average powers ratios.

III. A FULL-DUPLEX RADIO PROTOTYPE USING THE CMOS MAGNETLESS CIRCULATOR

In this section, we present the prototyped FD radio which consists of an antenna, an integrated non-magnetic CMOS circulator as described in Section II, a conventional frequency-flat amplitude- and phased-based RF SI canceller¹, and a USRP2 SDR. Fig. 2(a) shows the block diagram of the prototyped FD radio.

A. Design of the Conventional RF Canceller

The block diagram of the passive RF canceller is shown in Fig. 2(b). The 0.8–1.3 GHz RF canceller taps a reference signal at the output of the USRP TX port and performs SIC at the

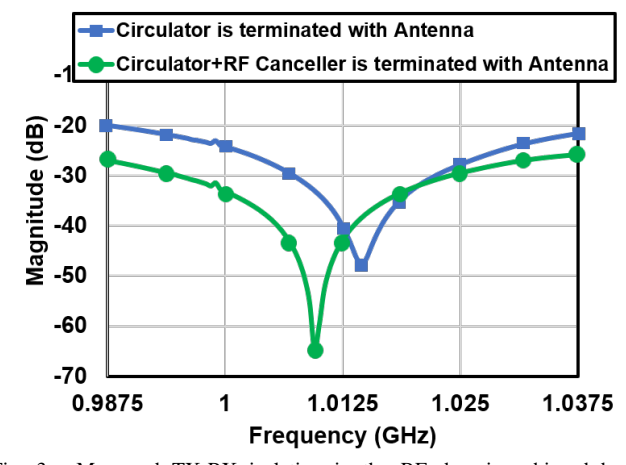


Fig. 3. Measured TX-RX isolation in the RF domain achieved by the circulator, and by circulator and the conventional RF canceller when the circulator ANT port is connected to a 1 GHz narrowband antenna.

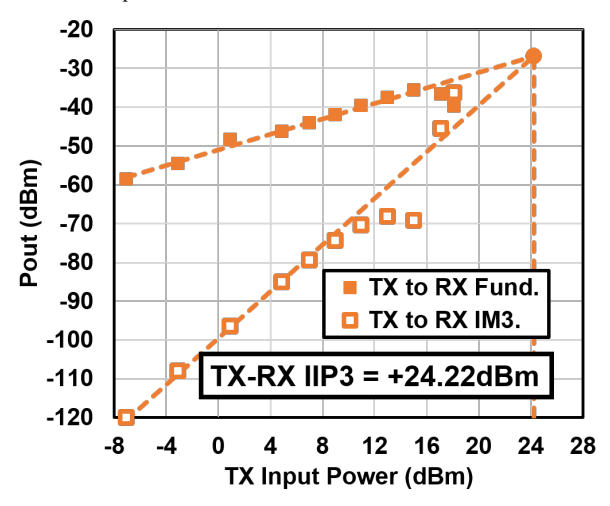
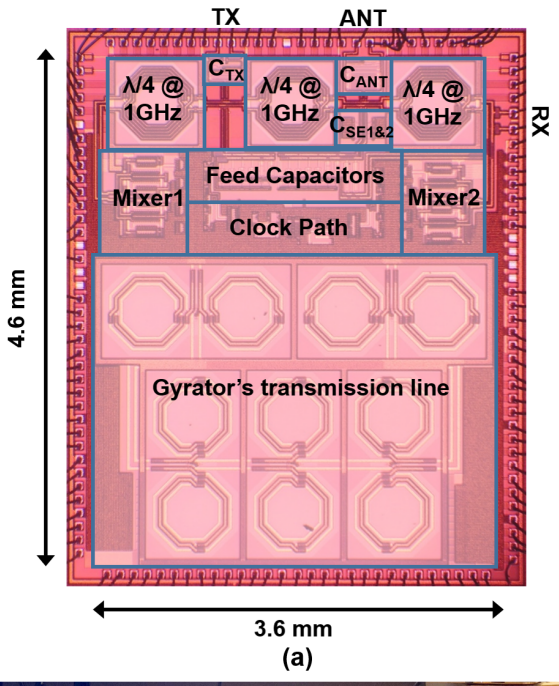


Fig. 4. Measured TX-RX IIP3 of the circulator when tuned for TX-RX isolation of $+50\,\mathrm{dB}$.

input of the USRP RX port. In particular, a portion of the TX signal is coupled from the output of the power amplifier (PA) through a 6 dB directional coupler. The TX reference signal is then adjusted in amplitude and phase by using an attenuator and a passive phase shifter, which are software-controlled from the laptop through a SUB-20 controller. The 5-bit attenuator provides an attenuation range from 0 dB to 15.5 dB with a 0.5 dB resolution. As a result, TX leakage between $-31\,\mathrm{dB}$ to $-15\,\mathrm{dB}$ (with respect to the absolute TX power levels) can be canceled. The passive phase shifter is controlled by an 8-bit digital-to-analog converter (DAC) and covers the full 360° range with a 1.5° resolution.

As mentioned in Section II, the isolation of the circulator can be tuned to $-55\,\mathrm{dB}$ using the switched capacitor banks. However, the maximum attenuation to the TX signal from the RF canceller is limited to $-31\,\mathrm{dB}$. Therefore, the RF canceller is configured to cancel the TX leakage from circulator at a small offset frequency from the circulator notch frequency as shown in Fig. 3. We also note that an RF canceller with larger attenuation range can potentially cancel the TX leakage from the circulator at its notch frequency, hence

¹An FD wireless link demo based on this conventional RF SI canceller was presented in [25]. An improved version of this RF SI canceller was integrated with then open-access ORBIT testbed for the research community to experiment with FD wireless [26].



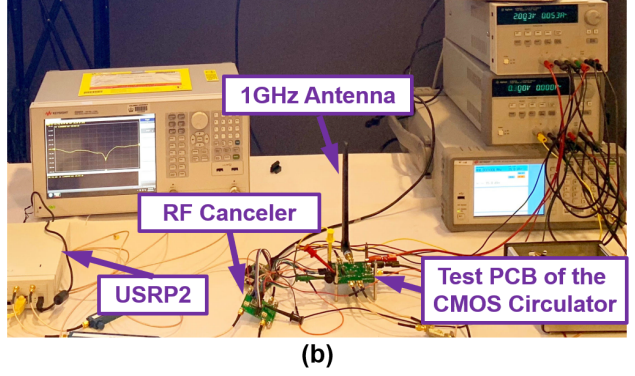


Fig. 5. (a) Chip microphotograph of the 1 GHz circulator implemented using 180 nm SOI CMOS technology. (b) Measurement setup of the FD radio prototype using CMOS circulator.

improving the TX-RX isolation. However, even with the current configuration, it can clearly be seen that the RF canceller increases the isolation as well as its bandwidth.

B. Digital SIC

The residual SI after circulator isolation and RF cancellation is further suppressed in the digital domain. The digital SI canceller is modeled as a truncated Volterra series [11], [16] and is implemented based on a non-linear tapped delay line to cancel both the main SI and the inter-modulation distortion generated on the SI. Specifically, the output of the discrete-time SI canceller, y_n , can be written as a function of the current and past TX digital baseband signals, x_n and x_{n-k} (k represents the delay index), i.e.,

$$y_n = \sum_{k=0}^{K} h_{1,k}(x_{n-k}) + \sum_{k=0}^{K} h_{2,k}(x_{n-k})^2 + \sum_{k=0}^{K} h_{3,k}(x_{n-k})^3,$$
(1)

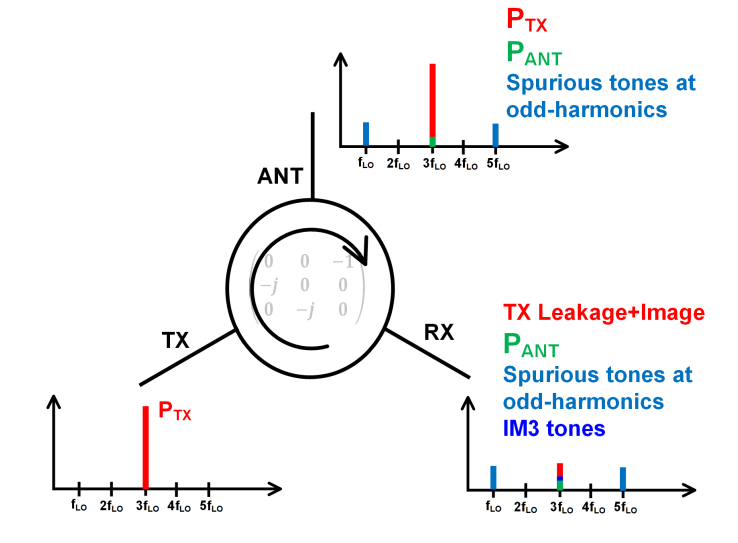


Fig. 6. Conceptual illustration of the spurious tone response of the circulator in presence of a strong transmitted signal $P_{\rm TX}$, received signal $P_{\rm RX}$ at the same frequency.

in which K corresponds to the maximum delay in the SI channel and $h_{m,k}$ (m=1,2,3) is the $m^{\rm th}$ order digital canceller coefficient. Depending upon the SI channel, higher order nonlinear terms can be included (the model in (1) only includes up to the $3^{\rm rd}$ -order non-linearity). Using a pilot data sequence, the digital SI canceller coefficients can be found by solving the least-square problem and is implemented in GNU Radio software.

C. Spurious Tone Response of the Periodically Time-Varying Circulator

Unlike time-invariant systems, time-varying systems should be characterized for their spurious tone responses as they can violate the spectral mask. We now qualitatively illustrate various spurious tones that can be created due to the clocking imperfections and non-linearity of the circulator. Let us consider the circulator operating in FD mode, with a signal $P_{\rm TX}$ at the TX port of the circulator at a frequency $f_{\rm TX}$ equal to $3f_{LO}$, and P_{ANT} at the ANT port of the circulator as shown in Fig. 6. The strong TX signal, P_{TX} , creates out-of-band spurious tones at the odd-harmonics of the clock², and an in-band image signal at the RX port of the circulator. Ideally, there should be no out-of-band spurious tones, but in practice they are present due to clocking imperfections. However, owing to the large offsets from the frequency of operation, these out-of-band spurious emissions can be heavily suppressed by using a filter between the antenna and the radio. Also, like all I/Q mixing systems, this circulator can be calibrated for image rejection, which would improve the suppression of the image tones to 50–60 dB so that they do not limit the circulator isolation. In addition, TX-RX non-linearity of the circulator results in in-band IM tones of the TX signal, at the RX port.

²Spurious tones near even-harmonics of the clock are suppressed due to the differential implementation of the circulator.

D. Effect of Circulator Non-Linearity on the SIC

At high TX powers, the TX-RX non-linearity of the circulator limits the maximum amount of SIC that can be achieved in an FD radio. For instance, the 3rd-order non-linearity of the circulator implies that the signal at the RX port of the circulator consists of TX signal (due to finite isolation of the circulator) along with its 3rd-order non-linear terms created by the circulator. These non-linear terms created by the circulator cannot be canceled in RF/analog domains as the portion of TX signal coupled into these cancellers does not contain the information of the non-linear terms created by the circulator, i.e., the RF/analog cancellers can only cancel the linear portion of the TX signal. However, these non-linear terms can be canceled in the digital domain using the non-linear tapped delay line model (see (1)). More significant non-linearity implies larger coefficients of the non-linear terms in (1). In the presence of the circulator non-linearity, the self-interference-to-noise ratio (XINR) of the FD radio, γ_{Self} , is given by

$$\gamma_{\rm Self} = \frac{P_{\rm SI,linear}^{\rm res} + P_{\rm SI,non-linear}^{\rm res}}{P_{\rm NF}} = \gamma_{\rm Self,linear} + \gamma_{\rm Self,non-linear},$$

where $P_{\rm SI,linear}^{\rm res}$ and $P_{\rm SI,non-linear}^{\rm res}$ are the power levels of the linear and non-linear components of the residual SI, respectively, with corresponding XINR values of $\gamma_{\rm Self,linear}$ and $\gamma_{\rm Self,non-linear}$.

Recall from Section II that the TX-RX IIP3 of the circulator when tuned for the maximum isolation of $+50\,\mathrm{dB}$ is $+24\,\mathrm{dBm}$ (see Fig. 4). The total SI power introduced by the 3^{rd} -order non-linearity at the RX port of the circulator, denoted by $P_{\mathrm{RX,IM3}}$, can be expressed in terms of TX power P_{TX} as

$$P_{\text{RX,IM3}} = (P_{\text{TX}} - 50) - 2 \times (24 - P_{\text{TX}}) = (3P_{\text{TX}} - 98) \,\text{dBm}.$$
 (2)

With a USRP noise floor of $P_{\rm NF}=-90\,{\rm dBm}$ for $10\,{\rm MHz}$ signal bandwidth³, a $+16\,{\rm dBm}$ TX signal would result in an non-linear SI power of $-90\,{\rm dBm}$ after digital SIC (i.e., $P_{\rm rx,IM3}-40\,{\rm dB}$ digital SIC with $P_{\rm TX}=+16\,{\rm dBm}$), which is equal to USRP receiver noise floor. Therefore, for TX power levels greater than+ $16\,{\rm dBm}$, $\gamma_{\rm Self}$ is degraded due to the non-linear components of the residual SI, which will lead to lower FD rate gains at the same link SNR value. In other words, better exploiting the watt-level power handling at the circulator TX port will require either improving circulator TX-RX IIP3 or better nonlinear digital cancellation algorithms.

IV. MEASUREMENTS

Fig. 5(a) shows the chip microphotograph of the CMOS circulator implemented in $180\,\mathrm{nm}$ SOI CMOS process, and Fig. 5(b) shows the measurement setup of the FD radio implemented using the CMOS circulator. A QPSK signal with $+15\,\mathrm{dBm}$ and $10\,\mathrm{MSa/s}$ sampling rate is provided at the TX of the circulator, and the SI spectra after the circulator isolation and RF cancellation, and after the digital cancellation

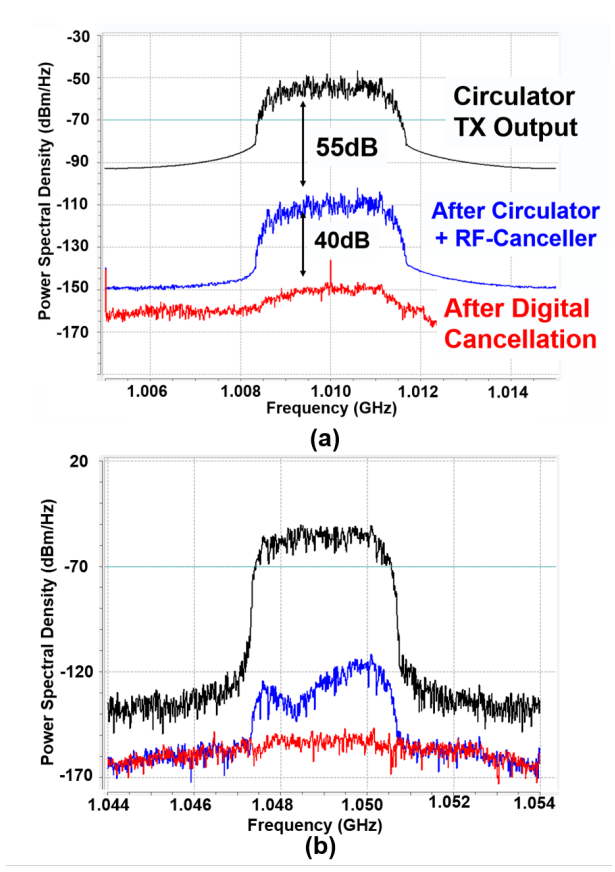


Fig. 7. Measured spectra of the received signal at the FD radio prototype at $+15\,\mathrm{dBm}$ TX power (a) with the 1 GHz CMOS circulator as descibed in Section II, and (b) with the 2^{nd} -generation 1 GHz CMOS circulator.

are shown in Fig. 7(a). The residual SI power ($P_{\rm SI,linear}^{\rm res} + P_{\rm SI,non-linear}^{\rm res}$) ≈ -80 dBm and the prototyped FD radio achieves an overall SIC of +95 dB across the antenna, RF, and digital domains. We note that using an analog domain canceller [23], [27] has the potential to achieve further improved SIC, and the overall SIC of the FD radio will be limited by the circulator TX-RX non-linearity. Fig. 7(b) shows the measured spectra when the $2^{\rm nd}$ circulator is used in the same FD radio. Here, +65 dB isolation is achieved using the circulator and the RF canceller, and the residual SI is further canceled to the USRP noise floor after the digital SIC.

Table I shows the corresponding FD rate gain computed using similar methods as described in [28], with experimentally measured XINR values of $\gamma_{\rm Self}=10\,{\rm dB}$ (Fig. 7(a)) and $\gamma_{\rm Self}=0\,{\rm dB}$ (Fig. 7(b)). We also account for the additional 3 dB link-loss due to the additional hardware in the FD radio, namely the CMOS circulator which features 5dB total loss in TX-ANT and ANT-RX paths, when compared to a typical TDD radio with a T/R switch that features 1dB loss in TX-ANT and ANT-RX paths each. The results show the relationship between the XINR, $\gamma_{\rm Self}$, with varying HD link SNR values. It can be seen that higher link SNRs and lower values of $\gamma_{\rm Self}$ will result in increased FD rate gain, but lower link SNRs and higher values of $\gamma_{\rm Self}$ can also possibly results in an FD rate gain of less than 1.

 $^{^3} This~USRP$ noise floor is the measured noise floor when an antenna is connected to the RX port. The true noise floor of the USRP is lower when the RX port is terminated with a $50~\Omega.$

TABLE I

FD rate gain computed using similar methods as described in [28], by taking the additional loss due to FD hardware (additional 3dB when compared to a traditional HD radio) into account along with experimentally measured $\gamma_{\rm Self}=10\,{\rm dB}$ (Fig. 7(a)) and $\gamma_{\rm Self}=0\,{\rm dB}$ (Fig. 7(b)).

HD Link SNR (dB)	0	10	20	30	40	50
$\gamma_{\text{Self}} = 10 \text{dB}$	0.13	0.31			1.33	1.46
$\gamma_{\text{Self}} = 0 \text{dB}$	0.65	1.05	1.41	1.60	1.70	1.76

V. CONCLUSION

In this work we present an FD radio which is implemented using a highly linear CMOS integrable magnetless circulator, an RF canceller and an USRP2 SDR. At a TX power level of +15 dBm, SIC of +55 dB has been achieved from circulator isolation and RF canceller, and an overall SIC of +95 dB is measured after the digital cancellation. We also analyzed the effects of TX-RX non-linearity on the overall SIC of FD radio. In addition, we also presented a qualitative discussion on the spurious response of the circulator in the FD operation in presence of a blocker. Improving the TX-RX nonlinearity of the circulator and adding an analog canceller to achieve even higher SIC is a topic of future research.

ACKNOWLEDGMENT

This work was supported in part by the DARPA SPAR program, and NSF grants ECCS-1547406, CNS-1650685, and CNS-1827923.

REFERENCES

- [1] A. Sabharwal, P. Schniter, D. Guo, D. W. Bliss, S. Rangarajan, and R. Wichman, "In-band full-duplex wireless: Challenges and opportunities," *IEEE J. Sel. Areas Commun.*, vol. 32, no. 9, pp. 1637–1652, 2014.
- [2] Z. Zhang et al., "Full duplex techniques for 5G networks: self-interference cancellation, protocol design, and relay selection," IEEE Commun. Mag., vol. 53, no. 5, pp. 128–137, 2015.
- [3] H. Krishnaswamy and G. Zussman, "1 chip 2x the bandwidth," *IEEE Spectrum*, vol. 53, no. 7, pp. 38–54, 2016.
- [4] J. Zhou et al., "Integrated full duplex radios," IEEE Commun. Mag., vol. 55, no. 4, pp. 142–151, 2017.
- [5] T. Chen, J. Diakonikolas, J. Ghaderi, and G. Zussman, "Hybrid scheduling in heterogeneous half-and full-duplex wireless networks," in Proc. IEEE INFOCOM'18, 2018.
- [6] G. Zheng et al., "Improving physical layer secrecy using full-duplex jamming receivers," *IEEE Trans. Signal Process.*, vol. 61, no. 20, pp. 4962–4974, 2013.
- [7] T. Riihonen, S. Werner, and R. Wichman, "Mitigation of loopback self-interference in full-duplex MIMO relays," *IEEE Trans. Signal Processing*, vol. 59, no. 12, pp. 5983–5993, 2011.
- [12] T. Chen et al., "Wideband full-duplex wireless via frequency-domain equalization: Design and experimentation," in Proc. ACM MobiCom'19 (to appear), 2019.

- [8] I. Krikidis, H. A. Suraweera, P. J. Smith, and C. Yuen, "Full-duplex relay selection for amplify-and-forward cooperative networks," *IEEE Trans. Wireless Commun.*, vol. 11, no. 12, pp. 4381–4393, 2012.
- [9] J. I. Choi, M. Jain, K. Srinivasan, P. Levis, and S. Katti, "Achieving single channel, full duplex wireless communication," in *Proc. ACM MobiCom'10*, 2010.
- [10] M. Duarte, C. Dick, and A. Sabharwal, "Experiment-driven characterization of full-duplex wireless systems," *IEEE Trans. Wireless Commun.*, vol. 11, no. 12, pp. 4296–4307, 2012.
- [11] D. Bharadia, E. McMilin, and S. Katti, "Full duplex radios," in *Proc. ACM SIGCOMM'13*, 2013.
- [13] J. Zhou, T. H. Chuang, T. Dinc, and H. Krishnaswamy, "Integrated Wideband Self-Interference Cancellation in the RF Domain for FDD and Full-Duplex Wireless," *IEEE J. Solid-State Circuits*, vol. 50, no. 12, pp. 3015–3031, Dec 2015.
- [14] B. van Liempd et al., "Adaptive RF Front-Ends Using Electrical-Balance Duplexers and Tuned SAW Resonators," *IEEE Transactions on Microwave Theory and Techniques*, vol. 65, no. 11, pp. 4621–4628, Nov 2017.
- [15] M. Chung et al., "Prototyping real-time full duplex radios," IEEE Commun. Mag., vol. 53, no. 9, pp. 56–63, 2015.
- [16] N. Reiskarimian et al., "A one-way ramp to a two-way highway: Integrated magnetic-free non-reciprocal antenna interfaces for full duplex wireless," *IEEE Microw. Mag.*, vol. 20, no. 2, pp. 56–375, 2019.
- [17] A. Nagulu, A. Alù, and H. Krishnaswamy, "Fully-Integrated Non-Magnetic 180nm SOI Circulator with >1W P1dB, >+50dBm IIP3 and High Isolation Across 1.85 VSWR," in 2018 IEEE Radio Frequency Integrated Circuits Symposium (RFIC), June 2018, pp. 104–107.
- [18] A. Kord, D. L. Sounas, and A. Alù, "Low-loss broadband magnetless circulators for full-duplex radios," in 2018 IEEE/MTT-S International Microwave Symposium - IMS, June 2018, pp. 506–509.
- [19] N. Reiskarimian, A. Nagulu, T. Dinc, and H. Krishnaswamy, "Nonreciprocal Electronic Devices: A Hypothesis Turned Into Reality," *IEEE Microw. Mag.*, vol. 20, no. 4, pp. 94–111, April 2019.
- [20] T. Dinc et al., "Synchronized Conductivity Modulation to Realize Broadband Lossless Magnetic-Free Non-Reciprocity," Nat. Commun., vol. 8, no. 765, Oct 2017.
- [21] A. Nagulu et al., "Nonreciprocal Components Based on Switched Transmission Lines," *IEEE Trans. Microw. Theory Techn.*, pp. 1–20, 2018.
- [22] B. D. H. Tellegen, "The Gyrator, A New Electric Network Element," Philips Res. Rep., vol. 3, no. 81, pp. 3003–3014, Dec 1948.
- [23] N. Reiskarimian, J. Zhou, and H. Krishnaswamy, "A CMOS Passive LPTV Nonmagnetic Circulator and Its Application in a Full-Duplex Receiver," *IEEE J. Solid-State Circuits*, vol. 52, no. 5, pp. 1358–1372, May 2017.
- [24] N. Reiskarimian et al., "Analysis and Design of Commutation-Based Circulator-Receivers for Integrated Full-Duplex Wireless," IEEE J. Solid-State Circuits, vol. 53, no. 8, pp. 2190–2201, Aug 2018.
- [25] T. Chen et al., "Demo: Full-duplex wireless based on a small-form-factor analog self-interference canceller," in Proc. ACM MobiHoc'16, 2016.
- [26] —, "Open-access full-duplex wireless in the ORBIT testbed," arXiv preprint arXiv:1801.03069, 2018.
- [27] T. Zhang et al., "Wideband Dual-Injection Path Self-Interference Cancellation Architecture for Full-Duplex Transceivers," IEEE J. Solid-State Circuits, vol. 53, no. 6, pp. 1563–1576, June 2018.
- [28] J. Marasevic et al., "Resource allocation and rate gains in practical full-duplex systems," *IEEE/ACM Trans. Netw.*, vol. 25, no. 1, pp. 292–305, 2017.